

Spectroscopic Identification, Structural Features and Molecular Docking Studies on 5-(4-Propoxybenzylidene)-2-[3-(4-chlorophenyl)-5-[4(propan-2-yl) phenyl]-4,5-dihydro-1H-pyrazol-1-yl]-1,3-thiazol-4(5H)-one using Pim-1 Kinase Cancer Protein

N. SHANMUGAPRIYA^{1,✉}, K. VANASUNDARI^{1,✉}, V. BALACHANDRAN^{1,*✉}, B. REVATHI^{1,✉}, C. SIVAKUMAR^{1,✉} and A. VIJ^{2,✉}

¹Centre for Research, Department of Physics, Arignar Anna Government Arts College (Affiliated to Bharathidasan University), Tiruchirappalli, Musiri-621211, India

²Kongunadu College of Engineering and Technology (Autonomous), Thottiam, Tiruchirappalli-621215, India

*Corresponding author: E-mail: brsbala@rediffmail.com

Received: 3 October 2021;

Accepted: 14 December 2021;

Published online: 10 March 2022;

AJC-20726

A comprehensive investigation of the molecular structure, electronic properties and vibrational spectra of 5-(4-propoxybenzylidene)-2-[3-(4-chlorophenyl)-5-[4-(propan-2-yl)phenyl]-4,5-dihydro-1H-pyrazol-1-yl]-1,3-thiazol-4(5H)-one have been studied. Many natural and/or synthetic compounds contain, thiazole which are attractive compounds found in the building of numerous natural products and certain pharmaceutical agents. To understand the molecular-orbital interaction and structural investigation of the title compound, the density functional theory (DFT) calculation has been carried out using B3LYP/6-31G and 6-311G basis sets combination. The experimental FT-IR, FT-Raman spectral data along with theoretical quantum chemical calculation were investigated. For potential energy distributions (PED) analysis, the VEDA 4 program is utilized to do comparative frequency assignments. With the optimized structures, the highest occupied molecular orbital (HOMO), the lowest unoccupied molecular orbital (LUMO) energies, molecular electrostatic potential (MEP) and natural bond orbital (NBO) were applied to describe the chemical reactivity. The electron density interactions distributed in space, which exist within these compounds are analyzed by different topological methods namely, atom in molecule (AIM), localized orbital locator (LOL), electron localization function (ELF) and the reduced density gradient (RDG). Finally, the molecular docking studies of the title compound for potent Pim-1 kinase cancer PDB ID: 3A99, 1GJ8, 1XQZ was investigated using the Auto Dock program.

Keywords: Thiazole, DFT, Atom in molecule, Reduced density gradient, Electron localization function, Pim kinase inhibitor.

INTRODUCTION

Heterocyclic aromatic compounds containing nitrogen and sulphur are the important molecules in organic chemistry synthesis [1,2]. Susithra *et al.* [3] reported when heterocycles are supposed to have hetero-nuclear atoms, they can be acted as an ideal ligand, which can delocalize and thereby stimulate resonance hybridization to interact with strong intermediate to produce the antimalarial drugs. The geometrical parameters such as bond length of 5-(4-propoxybenzylidene)-2-[3-(4-chlorophenyl)-5-[4-(propan-2-yl) phenyl]-4,5-dihydro-1H-pyrazol-1-yl]-1,3-thiazol-4(5H)-one have been obtained from B3LYP/6-31G and 6-311G basis sets. The global reactivity descriptors (ionization potential, electron affinity, electro-negativity, electrophilicity index, global hardness, global soft-

ness and chemical potential) has been predicted with the help of HOMO/LUMO energy values. Experimental FT-IR, FT-Raman spectra of the title compound were recorded and compared with the computed values obtained by the same level of DFT with B3LYP functional.

Chemically interactive regions in the molecule have been concentrated through aim in molecule (AIM), localized orbital locator (LOL), electron localization function (ELF) and reduced density gradient (RDG) [3]. Natural bond orbital (NBO) analysis has been performed to explain the conjugative interaction, donor, acceptor and second-order perturbation of the compound. Also, based on a key factor in PASS online data allows to define a variety of medicinal potential. Attract attention by repetition in listening data and then provide content of Pim-1 kinase inhibitors. The proto-oncogene proviral integration site for

Moloney murine leukemia virus (PIM) kinases (PIM-1, PIM-2 and PIM-3) are serine/threonine kinases that are involved in several signalling pathways important in cancer cells [4-6]. This investigation aimed to evaluate the role Pim kinase inhibitor in ligand progression using molecular docking.

EXPERIMENTAL

The synthesized compound 5-(4-propoxybenzylidene)-2-[3-(4-chlorophenyl)-5-[4-(propan-2-yl)phenyl]-4,5-dihydro-1H-pyrazol-1-yl]-1,3-thiazol-4(5H)-one has been taken without any further purification as per the procedure reported by Salian *et al.* [7] and spectroscopic grade for acquiring spectra. The FT-IR spectrum of the compound were recorded in Perkin-Elmer spectrometer fitted with a KBr beam splitter covering 4000-400 cm^{-1} region at a resolution of $\pm 1 \text{ cm}^{-1}$. The FT-Raman spectrum of the chosen compound was measured using Bruker RFS 27 model. The spectrum was recorded in the region 3500-0 cm^{-1} Stokes region using the 1064 nm line of a Nd:YAG laser for the excitation operating at 200 mW power.

Computational details

The DFT computational method is widely used to describe the quantum states of many-electron systems of the molecule. The Gaussian 09W [8] program package was utilized to proceed with DFT calculations on the title compound through, B3LYP/6-31G and B3LYP/6-311G basis sets to characterize the structure electronic and other properties. The geometrical parameter bond length has been obtained using B3LYP/6-31G and 6-311G basis sets [9]. Further, we have used the optimized ground state geometry of the title compound to study the different properties

like FT-IR, FT-Raman, MEP surface mapping and NBO analysis. The theoretical vibrational wavenumber obtained for compound is interpreted by means of potential energy distribution (PED %) calculations using VEDA4 software [10] Frontier molecular orbital (FMOs) analysis (HOMO-LUMO) and molecular electrostatic potential (MEP) with contour map have been performed by Gauss View 5.0 to obtain the electronic properties of the title compound. Multiwfn software [11] has also been utilized to obtain topology analysis (AIM, RDG, LOL and ELF). NBO analysis [12] provides an investigation of charge transfer or conjugative interactions in molecular systems, has been done using NBO 3.1 program available in Gaussian 09 package at DFT/6-311G level of theory. Besides, molecular docking studies were visualized using pymol and Discovery studio software [13,14]. The interactions of the title molecule with a Pim-1 kinase inhibitors PDB ID: 3A99, 1GJ8, 1XQZ receptors were studied.

RESULTS AND DISCUSSION

Molecular geometry: The optimized molecular structure of the title compound is shown in Fig. 1. The bond lengths of the title compound compared with a closely related crystallographic data available in literature [7] are presented in Table-1.

According to it, the C-H bond length observed at 1.08-1.10 Å for phenyl ring and 1.09 Å for pyrazol ring using a theoretical approach by B3LYP/6-31G and B3LYP/6-311G. Experimentally, the C-H bond in phenyl ring has a bond length range of 0.93 Å and 0.97-0.98 Å in pyrazol ring. This difference might be attributed due to fact that low scattering factor of hydrogen atom involved in the diffraction method [15]. The

TABLE-1
OPTIMIZED GEOMETRICAL PARAMETERS (BOND LENGTHS, Å) OF 5-(4-PROPOXYBENZYLIDENE)-2-[3-(4-CHLOROPHENYL)-5-[4-(PROPAN-2-YL)PHENYL]-4,5-DIHYDRO-1H-PYRAZOL-1-YL]-1,3-THIAZOL-4(5H)-ONE

Parameter	B3LYP/ 6-31G	B3LYP/ 6-311G	XRD	Parameter	B3LYP/ 6-31G	B3LYP/ 6-311G	XRD	Parameter	B3LYP/ 6-31G	B3LYP/ 6-311G	XRD
C ₁ -C ₄	1.46	1.46	1.46	C ₁₆ -H ₂₀	1.08	1.08	0.93	C ₄₂ -N ₄₃	1.30	1.30	1.30
C ₁ -N ₂₄	1.31	1.30	1.29	C ₁₇ -C ₂₁	1.41	1.41	1.38	C ₄₅ -C ₄₆	1.46	1.46	1.45
C ₁ -C ₂₆	1.52	1.52	1.50	C ₁₇ -H ₂₂	1.09	1.08	0.93	C ₄₅ -H ₅₆	1.09	1.09	0.93
C ₂ -C ₁₄	1.52	1.52	1.51	C ₁₉ -C ₂₁	1.40	1.40	1.39	C ₄₆ -C ₄₇	1.42	1.41	1.39
C ₂ -N ₂₅	1.51	1.51	1.51	C ₁₉ -H ₂₃	1.09	1.08	0.98	C ₄₆ -C ₄₈	1.42	1.42	1.39
C ₂ -C ₂₆	1.56	1.56	1.47	C ₂₁ -C ₂₉	1.53	1.53	1.52	C ₄₇ -C ₄₉	1.39	1.39	1.38
C ₂ -H ₅₅	1.09	1.09	0.98	N ₂₄ -N ₂₅	1.39	1.39	1.38	C ₄₇ -H ₅₀	1.09	1.08	0.93
H ₃ -C ₂₆	1.09	1.09	0.97	N ₂₅ -C ₄₂	1.35	1.35	1.34	C ₄₈ -C ₅₁	1.39	1.39	1.37
C ₄ -C ₅	1.41	1.41	1.38	C ₂₆ -H ₂₈	1.10	1.09	0.97	C ₄₈ -H ₅₂	1.08	1.08	0.93
C ₄ -C ₆	1.41	1.41	1.40	C ₂₉ -C ₃₀	1.55	1.54	1.41	C ₄₉ -C ₅₃	1.40	1.40	1.38
C ₅ -C ₇	1.40	1.40	1.37	C ₂₉ -C ₃₁	1.55	1.54	1.41	C ₄₉ -H ₅₇	1.08	1.08	0.93
C ₅ -H ₈	1.08	1.08	0.93	C ₂₉ -H ₃₈	1.10	1.09	0.96	C ₅₁ -C ₅₃	1.41	1.40	1.36
C ₆ -C ₉	1.39	1.39	1.37	C ₃₀ -H ₃₂	1.10	1.09	0.96	C ₅₁ -H ₅₄	1.08	1.08	0.93
C ₆ -H ₁₀	1.08	1.08	0.93	C ₃₀ -H ₃₃	1.10	1.09	0.96	C ₅₃ -O ₅₈	1.38	1.39	1.37
C ₇ -C ₁₁	1.39	1.39	1.36	C ₃₀ -H ₃₄	1.10	1.09	0.96	O ₅₈ -C ₅₉	1.46	1.46	-
C ₇ -H ₁₂	1.08	1.08	0.93	C ₃₁ -H ₃₅	1.10	1.09	0.96	C ₅₉ -H ₆₀	1.10	1.09	-
C ₉ -C ₁₁	1.40	1.39	1.38	C ₃₁ -H ₃₆	1.10	1.09	0.96	C ₅₉ -H ₆₁	1.10	1.09	-
C ₉ -H ₁₃	1.08	1.08	0.93	C ₃₁ -H ₃₇	1.10	1.09	0.96	C ₅₉ -C ₆₂	1.52	1.52	-
C ₁₁ -C ₁₇	1.82	1.83	1.78	C ₃₉ -C ₄₀	1.49	1.49	1.50	C ₆₂ -H ₆₃	1.10	1.09	-
C ₁₄ -C ₁₅	1.41	1.40	1.37	C ₃₉ -S ₄₁	1.87	1.87	1.75	C ₆₂ -H ₆₄	1.10	1.09	-
C ₁₄ -C ₁₆	1.40	1.40	1.37	C ₃₉ -C ₄₅	1.36	1.36	1.34	C ₆₂ -C ₆₅	1.54	1.54	-
C ₁₅ -C ₁₇	1.40	1.39	1.38	C ₄₀ -N ₄₃	1.41	1.41	1.38	C ₆₅ -H ₆₆	1.09	1.09	-
C ₁₅ -H ₁₈	1.09	1.08	0.93	C ₄₀ -O ₄₄	1.25	1.25	1.22	C ₆₅ -H ₆₇	1.10	1.09	-
C ₁₆ -C ₁₉	1.40	1.40	1.39	S ₄₁ -C ₄₂	1.84	1.84	1.76	C ₆₅ -H ₆₈	1.10	1.09	-

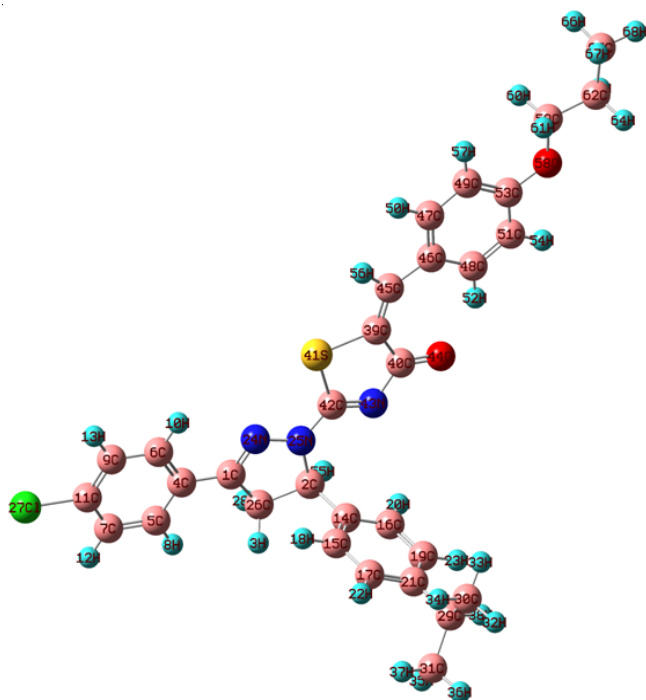


Fig. 1. Optimized structure of 5-(4-propoxybenzylidene)-2-[3-(4-chlorophenyl)-5-[4(propan-2-yl)phenyl]-4,5-dihydro-1H-pyrazol-1-yl]-1,3-thiazol-4(5H)-one

C-C bond lengths in all rings lie between the normal C-C single and C=C double bond lengths indicating the conjugation of electron density in all the ring [16]. It shows that the varied range of C-C bond length of 1.36 Å to 1.55 Å for B3LYP/6-31G/6-311G and 1.29 Å to 1.52 Å for XRD, respectively.

The intermolecular distance of C₂-C₂₆ (1.56 Å/DFT, 1.54 Å/XRD) is higher than the other C-C atoms. This is due to the presence of a nitrogen atom (N₂₅) that attached to the C₂ atom. The pyrazol ring C-N bond lengths are C₂-N₂₅ = 1.51 Å /DFT, 1.47 Å/XRD. The C-N values in the thiazol ring, show that the bond lengths for C₄₂-N₄₃ is 1.30 Å in both DFT/XRD and C₄₀-N₄₃ are 1.41 Å/DFT and 1.38 Å/XRD. Likewise, C-S values of thiazole ring C₃₉-S₄₁ and S₄₁-C₄₂ bond lengths are 1.87 Å and 1.84 Å, respectively. These values suggest that some multiple bond character is present in the thiazole ring [17]. The C=O bond lengths (DFT/XRD) in the carbonyl group are 1.26 Å (C-O) reported by Mary [18]. Similarly, the C₄₀=O₄₄ bond showed double bond character, with a bond length value of 1.25 Å by both B3LYP/6-31G/B3LYP/6-311G and 1.22 Å in XRD. The bond lengths of propoxybenzylidene in the title compound are C₆₂-C₆₅ = 1.65 Å/DFT, O₅₈-C₅₉ = 1.46 Å/DFT, C₅₃-O₅₈ = 1.39 Å/DFT comparable to that reported value [19].

Normally, the C-Cl bond length indicates a considerable increase in its length when compared with the C-H bond length [15]. Experimental value relates to the chlorine atom substituted phenyl ring shown the bond length 1.78 Å. From this observation, it is clear that the C₁₁-Cl₂₇ bond length of the title compound falls at 1.82 Å and 1.83 Å using B3LYP/6-31G and 6-311G. The comparative analysis reveals that except of few values observed in DFT, calculated bond lengths are good agreement with literature values.

Vibrational assignments: In recent years, FT-IR and FT-Raman have been mostly used as vibrational spectroscopy for structural characterization of molecular systems through DFT calculations. The title compound is constituted by N = 68 atoms and hence has $3N-6 = 198$ normal modes of vibration. The observed and calculated wavenumber and potential energy distributions are discussed below. The fundamental modes of vibration were carried out and are depicted in Table-2. The simulated and experimental FT-IR and FT-Raman spectra are given in Figs. 2 and 3, respectively.

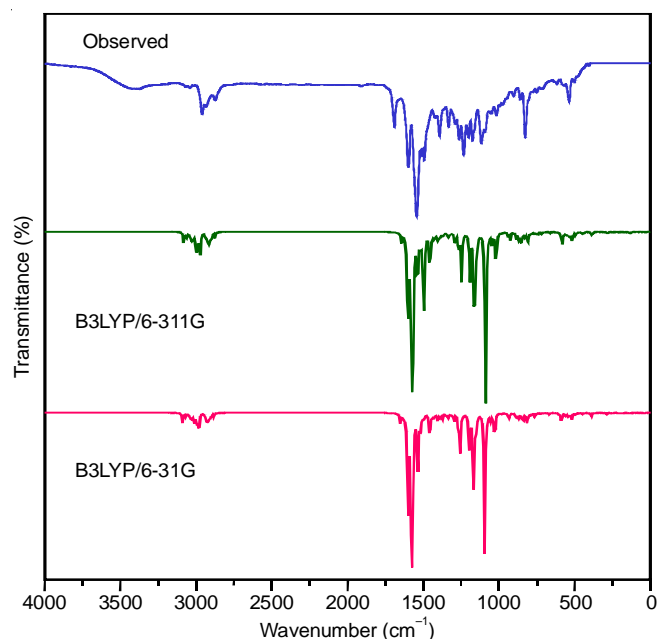


Fig. 2. FT-IR simulated spectra of 5-(4-propoxybenzylidene)-2-[3-(4-chlorophenyl)-5-[4(propan-2-yl)phenyl]-4,5-dihydro-1H-pyrazol-1-yl]-1,3-thiazol-4(5H)-one

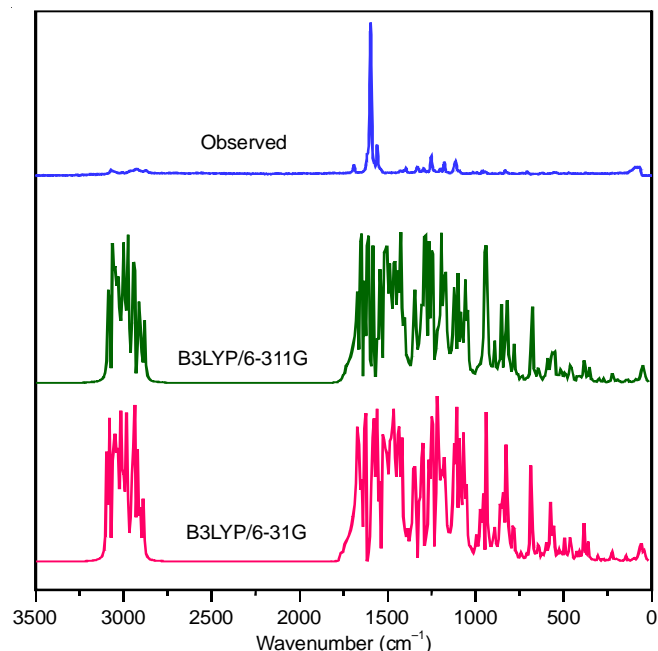


Fig. 3. FT-Raman simulated spectra of 5-(4-propoxybenzylidene)-2-[3-(4-chlorophenyl)-5-[4(propan-2-yl)phenyl]-4,5-dihydro-1H-pyrazol-1-yl]-1,3-thiazol-4(5H)-one

TABLE-2
 VIBRATIONAL ASSIGNMENTS, OBSERVED AND CALCULATED WAVENUMBERS (cm⁻¹) OF 5-(4-PROPOXYBENZYLIDENE)-
 2-[3-(4-CHLOROPHENYL)-5-[4-(PROPAN-2-YL) PHENYL]-4,5-DIHYDRO-1H-PYRAZOL-1-YL]-1,3-THIAZOL-4(5H)-ONE
 AT B3LYP METHOD WITH 6-31G AND 6-311G BASIS SETS

Observed wavenumbers (cm ⁻¹)		Calculated wavenumbers (cm ⁻¹) (scaled)		Vibrational assignments (PED%)	Observed wavenumbers (cm ⁻¹)		Calculated wavenumbers (cm ⁻¹) (scaled)		Vibrational assignments (PED%)	
FT-IR	FT-Raman	B3LYP/6-31G	B3LYP/6-311G		FT-IR	FT-Raman	B3LYP/6-31G	B3LYP/6-311G		
3070w		3091	3082	vCH(99)	1050w		1055	1051	δring (61)	
		3075	3070	vCH(99)			1050	1042	δring (61)	
		3070	3066	vCH(98)			1036	1030	δring (60)	
		3066	3060	vCH(98)			1029	1023	γCH(58)	
		3061	3054	vCH(98)		1017ms		1024	1016	vCO (69), vCC (12)
3040w		3053	3049	vCH(99)			1014	1009	γCH(59)	
		3045	3042	vCH(98)	1000w			1006	1002	γCH(59)
		3040	3036	vCH(98)				1003	998	γCH(60)
		3037	3031	vCH(99)				983	982	γCH(60)
		3031	3028	vCH(99)		975w		979	973	γopr CH ₃ (62)
	3027	3023	vCH(98)				965	961	γCH(58)	
2936w		3024	3019	vCH(98)	950vw			955	950	vCS(74)
		3018	3014	vCH(99)				946	943	γopr CH ₃ (62)
		3012	3008	v _{ass} CH ₃ (97)				939	938	γCH(58)
		3009	3002	v _{ass} CH ₃ (97)			929	925	δring (61)	
		3000	2996	v _{ass} CH ₂ (98)			921	917	γCH ₃ (60)	
2961ms		2996	2991	v _{ass} CH ₃ (97)	904w	900	908	903	δrock CH ₃ (61)	
		2990	2985	v _{ass} CH ₂ (97)				895	891	δrock CH ₃ (61)
		2981	2977	v _{ass} CH ₃ (97)				886	882	γCH(58)
		2975	2970	vCH(98)				878	875	γCH(58)
		2970	2963	v _{ass} CH ₃ (97)				870	866	γCH(58)
2936w		2951	2945	v _{ass} CH ₃ (97)	860w		868	860	γCH(58)	
		2942	2938	v _{ss} CH ₂ (98)			856	854	γCH(57)	
		2933	2930	v _{ass} CH ₃ (97)			845	841	γCH(58)	
		2930	2924	v _{ss} CH ₂ (98)		827w	832w	834	830	Ring breathing (60)
		2925	2919	v _{ss} CH ₃ (98)					818	815
	2918	2912	v _{ss} CH ₃ (98)		809			806	γCS(75)	
	2909	2903	v _{ss} CH ₃ (98)		796			792	γCS(74)	
	2901	2896	vCH(97)		790			785	δring (64)	
2875m		2882	2875	v _{ss} CH ₂ (98)		782	778	δwagg CH ₂ (61)		
1692ms		1650	1643	vCO (71), vCN (21)		769	765	δCO(70)		
		1631	1625	vCC (68), δCH (19)	756w		763	759	γCO(68)	
		1619	1614	vCC (68), δCH (20)			750	743	γring (56)	
		1606	1604	vCC (68), δCH (20)			725	721	γring (55)	
	1599s	1596vs	1599	1599		vCC (67), vCN (15), δCH (12)	720w		720	716
1596			1592	vCC (67), vCN (15), δCH (10)				706	702	γring (55)
1585			1581	vCC (68), δCH (13), δCC (10)		692		689	vCC(66)	
1579			1576	vCN (66), vCO (13), vCC (12)		666		662	δipr CH ₃ (59)	
1572			1570	vCC (68), δCO (16), vCN (10)		648		643	δccl(57)	
1542vs	1560s	1566	1564	vCN (69), vCO (19)		629	626	γCH(58)		
		1551	1551	δCH (72), vCC (10)	618w		620	617	γCH(58)	
		1540	1542	ρ _{sciss} CH ₂ (76)			600	596	γCH(59)	
		1534	1535	δCH (73), vCC (12)			585	581	γCH(58)	
		1530	1527	δCH (65), vCC (17)		569w		579	572	γCH(58)
1521	1519	δopbCH ₃ (6a)		566			560	γCH(58)		
1514	1511	δopbCH ₃ (69)		554	551		Ring breathing (60)			
1506	1503	δopbCH ₃ (68)	536w		538		535	γCH(59)		
1494ms		1496		1495	δipbCH ₃ (68)			531	525	γring (54)
		1494		1490	ρ _{sciss} H ₂ (75)		517	513	δring (55)	
		1485		1483	δipbCH ₃ (68)	504w		505	501	δring (55)
		1475		1475	δipbCH ₃ (68)			494	490	δCC (61)
		1466	1462	ρ _{sciss} H ₂ (75)			475	472	δCC (60)	
		1456	1456	δCH (68), vCC (10)			461	453	γCC (52)	
		1453	1450	δCH (68), vCC (12)			446	441	γCO (50)	
1494ms	1440w	1445	1441	δsb CH ₃ (76)		440	438	γCH (54)		
		1438	1435	δsb CH ₃ (76)		435	430	γring (54)		
		1431	1426	δCH (68)		422	419	γring (54)		

1423ms		1420	1417	δ CH (68)	406vw	412	408	γ ring (54)
		1413	1408	δ sb CH ₃ (75)		406	400	γ CC (55)
	1400m	1403	1400	vCN (66), δ CH (14)		388	385	γ ring (49)
		1389	1389	σ rock CH ₂ (67), vCC (16)		373	372	γ CCl (51)
		1380	1381	δ CH (65), vCCC (12)		364	360	δ ring (50)
		1376	1375	vCC (65), δ CH (10)		350	345	γ CC (48)
		1370	1368	δ CH (66), vCCC (12)		339	333	γ CCH ₃ (49)
		1355	1353	δ CH (66)		320	316	δ CC (54)
		1348	1344	σ rock (65), vCCC (10)		306	301	δ CC (55)
	1330m	1336	1335	δ CH (65), vCCC (12)		284	280	δ ring (60)
		1330	1327	vCC (63), δ CH (12)		279	274	δ CC (58)
		1316	1313	vCC (68), δ CH (13)		256	252	τ CCH ₃ (54)
		1304	1302	δ CH (66)		250	246	δ CC (58)
1288ms	1288m	1294	1290	σ rock CH ₂ (67), vCC (12)		248	241	τ CH ₃ (48)
		1285	1283	τ CH ₂ (59)		235	230	τ CH ₃ (48)
		1275	1271	vCC (63), δ CH (23)		229	225	τ CH ₃ (48)
1264ms		1266	1263	δ CH (68)		222	217	δ ring (57)
		1261	1257	σ rock CH ₂ (67)		214	208	γ CO (61)
		1253	1250	δ CH (68)		206	202	δ ring (59)
	1245ms	1245	1243	τ CH ₂ (58)		200	196	δ ring (60)
1233s		1234	1235	vCC (66), δ CH (14)		183	175	γ CO (57)
		1232	1228	δ CH (63), vCCC (16)		174	168	δ ring (58)
		1223	1220	δ CH (65)		161	155	γ CC (49)
		1216	1212	δ CH (65), vCCC (12)		148	140	γ CO (48)
		1205	1203	δ CH (66)		135	130	γ CN (48)
		1194	1190	δ CH (65)		125	119	δ ring (53)
		1190	1188	δ CH (66)		106	98	δ ring (55)
1180ms		1186	1182	τ CH ₂ (57)		95	87	τ CO (49)
1175ms	1175ms	1175	1171	γ wagg CH ₂ (55)	78vw	89	80	γ CC (49)
		1166	1160	δ CO (61)		83	73	γ CC (48)
		1156	1153	δ CH (66)		75	67	γ CC (49)
		1147	1144	δ CH (64)		62	56	δ CC (58)
		1143	1139	δ CH (64)		55	49	δ CC (58)
	1125ms	1132	1127	δ CH (64)		49	40	γ ring (48)
		1115	1112	vCCH ₃ (67)		45	36	γ CC (48)
		1099	1096	δ ring (60)		39	31	γ CC (47)
1092ms		1094	1092	vCCH ₃ (66)		35	28	γ CC (48)
		1091	1085	vNN (72), δ CN (14), δ CO (10)		31	25	γ CC (48)
		1086	1081	vCC (67), δ ring (16)		26	22	γ CC (48)
		1080	1075	vCC (68), vCO (14)		21	19	γ CC (45)
		1071	1066	γ CH (59)		16	14	γ CC (45)
		1064	1060	δ ring (61)		9	6	γ CC (48)

C–H vibrations: The hetero-aromatic structure shows the presence of C–H stretching vibrations in the region of 3100–3000 cm^{-1} [20]. The characteristic region for the identification of the C–H stretching vibration is affected by the nature of substituent group interaction. In present study, the C–H stretching vibrations are observed at 3040 cm^{-1} and 3070 cm^{-1} in the FT-IR spectrum. The scaled frequency of C–H stretching bands have been obtained from 3091–3018 cm^{-1} using B3LYP/6-31G and 3082–3014 cm^{-1} using B3LYP/6-311G basis set. The hetero-aromatic configuration reveals the presence of C–H stretching, in-plane and out-of-plane bending vibrations in the range 3200–3000 cm^{-1} , 1200–900 cm^{-1} and 980–700 cm^{-1} . Substitution sensitive C–H in-plane-bending vibrations are in the range of 1300–1000 cm^{-1} [21]. In the title compound, the medium strong bands at 1264 cm^{-1} in the FT-IR spectrum and at 1125 cm^{-1} in the FT-Raman spectrum were assigned as C–H in-plane-bending vibrations. The theoretically computed wavenumbers for this mode were 1266, 1261, 1205, 1194, 1190, 1156, 1147, 1143

and 1132 cm^{-1} using B3LYP/6-31G and at 1263, 1257, 1203, 1190, 1118, 1153, 1144, 1139 and 1127 cm^{-1} using B3LYP/6-311G. The C–H out-of-plane bending vibrations are observed as a weak band at 994, 860, 618, 569 and 536 cm^{-1} in FT-IR and at 1000 and 950 cm^{-1} in FT-Raman spectra, respectively. The calculated frequencies of these modes are in the range of 1014–983 cm^{-1} , 886–845 cm^{-1} and 629–538 cm^{-1} using B3LYP/6-31G and at 1009–982 cm^{-1} , 882–841 cm^{-1} and 626–535 cm^{-1} using a B3LYP/6-311G basis set. Thus, the theoretically evaluated values for C–H vibrational modes are in good agreement with the experimental data.

CH₃ vibrations: Generally, there are nine fundamental modes of vibrations associated in CH₃ groups such as symmetrical stretch, two asymmetrical stretch, in-plane bending, out-of-plane bending, symmetric bending, in-plane rocking, out-of-plane rocking and twisting [22]. Asymmetric and symmetric stretching modes of a methyl group attached to the benzene ring are usually downshifted because of electronic effects and

are expected near 2925 and 2865 cm^{-1} for asymmetric and symmetric stretching vibrations. The CH_3 stretching modes are reported at 2980, 2917, 2895 cm^{-1} in the IR spectrum, 2987, 2980, 2916, 2899 cm^{-1} in the Raman spectrum are assigned by Viji *et al.* [23]. In the title compound, the CH_3 asymmetric and symmetric stretching modes appear in the range 3012–2920 cm^{-1} ; 2930–2909 cm^{-1} by B3LYP/6-31G and 3008–2963 cm^{-1} and 2924–2903 cm^{-1} by B3LYP/6-311G method. The in-plane bending vibrations of the CH_3 group were experimentally obtained at 1494 cm^{-1} FT-IR spectrum and 1440 cm^{-1} in FT-Raman spectrum and these values are in good agreement with the literature [24]. In the present study, the calculated out-of-plane and in-plane bending vibration were located in the region 1521–1438 cm^{-1} (6-31G) and 1519–1435 cm^{-1} (6-311G). Out of three, only two in-plane rocking deformations at 904 cm^{-1} in FT-IR and 900 cm^{-1} in FT-Raman spectra are in agreement with theoretical values 908, 895 cm^{-1} by B3LYP/6-31G and 903, 891 cm^{-1} by B3LYP/6-311G, respectively. The computed twisting τCH_3 values by B3LYP/6-31G method are predicted at $\tau = 256, 248, 235, 229 \text{ cm}^{-1}$ and 252, 241, 230, 225 cm^{-1} by B3LYP/6-311G level of theory (Table-2).

CH_2 vibrations: There are six fundamental modes of vibrations can be associated with the CH_2 group, namely asymmetric and symmetric stretching, scissoring and rocking (in-plane bending), wagging and twisting (out-of-plane bending). Arjunan *et al.* [25] reported the symmetric methylene group stretching vibration observed at 2922 cm^{-1} . In this investigation, the CH_2 symmetric stretching mode observed at 2936 cm^{-1} in FT-IR spectrum and the theoretical value appears at 2942 cm^{-1} by B3LYP/6-31G and 2938 cm^{-1} by B3LYP/6-311G method. For, asymmetric stretch $\nu_{\text{ass}}\text{CH}_2$ was predicted theoretically at 3000, 2990 cm^{-1} by B3LYP/6-31G and 2996, 2985 cm^{-1} by B3LYP/6-311G. The rocking (σ_{rock}) mode is assigned at 1288 cm^{-1} in both FT-IR and FT-Raman spectra and at 1294 (6-31G), 1290 (6-311G) cm^{-1} theoretically (B3LYP).

The CH_2 wagging (γ_{wagg}) mode is observed at 1175 cm^{-1} in both FT-IR and FT-Raman spectra and theoretically the values obtained at 1175(6-31G), 1171(6-311G) cm^{-1} . The twisting mode of CH_2 vibration is identified at 1180 cm^{-1} in the FT-IR spectrum and 1245 cm^{-1} in FT-Raman spectrum. The DFT calculated frequencies are observed at 1245, 1186 cm^{-1} by B3LYP/6-31G and at 1233, 1182 cm^{-1} by B3LYP/6-311G.

C–C vibrations: In phenyl ring, carbon-carbon stretching vibrations are usually appear in the interval of 1625–1400 cm^{-1} [26–28]. In the present study, the DFT calculated frequencies are observed in the range 1631–1585 cm^{-1} using B3LYP/6-31G and 1625–1581 cm^{-1} using B3LYP/6-311G basis set. The same modes strong peaks are observed in FT-Raman spectrum at 1596 (vs) cm^{-1} and in FT-IR spectrum at 1599(s) cm^{-1} . Normally, the ring deformation modes are observed below the frequency 1000 cm^{-1} . Shankar Rao *et al.* [27] calculated the in-plane C–C–C deformation bands occur in the region at 651–509 cm^{-1} while the out-of-plane C–C–C deformation bands occur in the region 477–282 cm^{-1} . Likewise, the C–C in-plane bending vibrations are obtained at 494, 475 cm^{-1} by B3LYP/6-31G and 490, 472 cm^{-1} by B3LYP/6-311G. The frequencies observed in the out-of-plane C–C bending vibration are experimentally at 78

cm^{-1} in FT-IR spectra. Here, the theoretical frequencies are assigned at in the region 89–90 cm^{-1} using B3LYP/6-31G and 80–86 cm^{-1} using B3LYP/6-311G.

C=O and C–O vibrations: In present investigation, the oxygen substitution were observed with C4(C_{40}) position of thiazole and aromatic substitution at the *para*-position of benzene (oxybenzylidene). The measurement of the C–O band is difficult due to the interfering with many other vibrations. Although there is a high absorption peak for CO vibrations when combined with C–C stretching, C–N stretching and C–H bending vibrations, the contribution of PED is only 20%. The C=O stretching vibration exhibits a strong band in the region 1750–1600 cm^{-1} and C–O stretching vibrations are in the region 1300–100 cm^{-1} [29]. On comparing the present investigation with the above literature, the medium strong band stretching mode of C=O is assigned at 1692 cm^{-1} and C–O is assigned at 1017 cm^{-1} in the FT-IR spectrum. The theoretical frequencies (B3LYP/6-31G) are 1650, 1024 cm^{-1} and 1643, 1016 cm^{-1} for B3LYP/6-311G.

C–Cl vibrations: Generally, the C–Cl in-plane (δ) and out-of-plane (γ) bending vibrations appears in the lower frequency region. Because the chlorine atom has a higher electronegativity than the carbon atom, the bonding electrons in the C–Cl bond will be closer to the chlorine than the carbon, increasing the force constant and causing a frequency shift [28]. In present study, the predicted in-plane (δ) bending vibrations is assigned at $\delta = 648 \text{ cm}^{-1}$ for B3LYP/6-31G and $\delta = 643 \text{ cm}^{-1}$ for B3LYP/6-311G. The out-of-plane (γ) bending vibrations have been assigned at $\gamma = 818, 373 \text{ cm}^{-1}$ for B3LYP/6-31G and $\gamma = 815, 372 \text{ cm}^{-1}$ for B3LYP/6-311G by theoretically.

C–S vibrations: The assignment of the molecular identification in C–S stretching vibrational mode is a difficult task. The absorption of this group having variable intensity, which can be found in a wide range of 1035–245 cm^{-1} in both aliphatic and aromatic sulphides [30]. The title compound were detected experimentally at 950 cm^{-1} in FT-Raman. Theoretically, the stretching of C–S band in the thiazol ring at 995 cm^{-1} in B3LYP/6-31G and 950 cm^{-1} in B3LYP/6-311G. The C–S out-of-plane bending vibration was observed at 809, 796 cm^{-1} by B3LYP/6-31G and 806, 792 cm^{-1} in B3LYP/6-311G.

C=N, C=N and N–N vibrations: In general, identifying C=N and C–N vibrations was particularly challenging because mixing of several bands appeared possible in this region. Silverstain *et al.* [31] reported the C–N stretching absorption in the region 1689–1417 cm^{-1} for aromatic compound. Similarly, computed value is agreeing with the literature. When C=N stretching band is found experimentally at 1400 cm^{-1} in FT-Raman, theoretically assignment at 1403 cm^{-1} in the B3LYP/6-31G and 1400 cm^{-1} B3LYP/6-311G. The theoretically computed N–N stretching vibration combined with C–N in-plane bending vibration has been calculated at 1091(6-31G) cm^{-1} , 1085(6-31G) cm^{-1} [32], respectively.

Global reactivity descriptors: The highest occupied molecular orbitals (HOMO) and lowest unoccupied molecular orbitals (LUMO) are fundamentally standard in quantum estimation; also, orbitals are called frontier molecular orbitals (FMOs). The FMOs portrays the molecular stability and it plays

a significant role in computing the molecular electrical transport properties. The E_{HOMO} and E_{LUMO} are frequently illustrating contour stabilization of the compounds by green-red isosurface circles, which clearly explain the charge transfer mechanism. The combination between these orbitals is important in various responses to describe the kinetic stability and chemical reactivity for the examined compounds. In present analysis, it is found that the title compound has a total of 600 orbitals out of which 143 are occupied and the remaining 457 are virtual orbitals. The orbitals numbered 143 and 144 account for HOMO and LUMO orbitals. The FMOs energy gap of studied molecule of B3LYP/6-31G basis set is reported as HOMO = -5.5198 eV, LUMO = -2.1701 eV, energy gap $\Delta E = -3.3497$ eV and B3LYP/

6-311G basis set is reported as HOMO = -5.7563 eV, LUMO = -2.3943 eV, energy gap $\Delta E = -3.3620$ eV. Taking higher basis set B3LYP/6-311G band gap energy values (H-1 \rightarrow L+1, H-2 \rightarrow L+2) of compound are found to be -4.5226 eV and -5.7234 eV (Fig. 4), respectively. The ionization potential $I = -E_{\text{HOMO}}$ with electron affinity $A = -E_{\text{LUMO}}$, electro-negativity $\chi = (I + A)/2$, chemical potential $\mu = -(I + A)/2$ with hardness $\eta = (I - A)/2$, softness $\sigma = 1/\eta$, electrophilicity index $\omega = \mu^2/2\eta$ of the title compound have been estimated theoretically [33] and the corresponding values are shown in Table-3.

Molecular electrostatic potential (MEP): MEP is related to the visualized map of electron density and is a very useful tool in understanding sites for electrophilic and nucleophilic

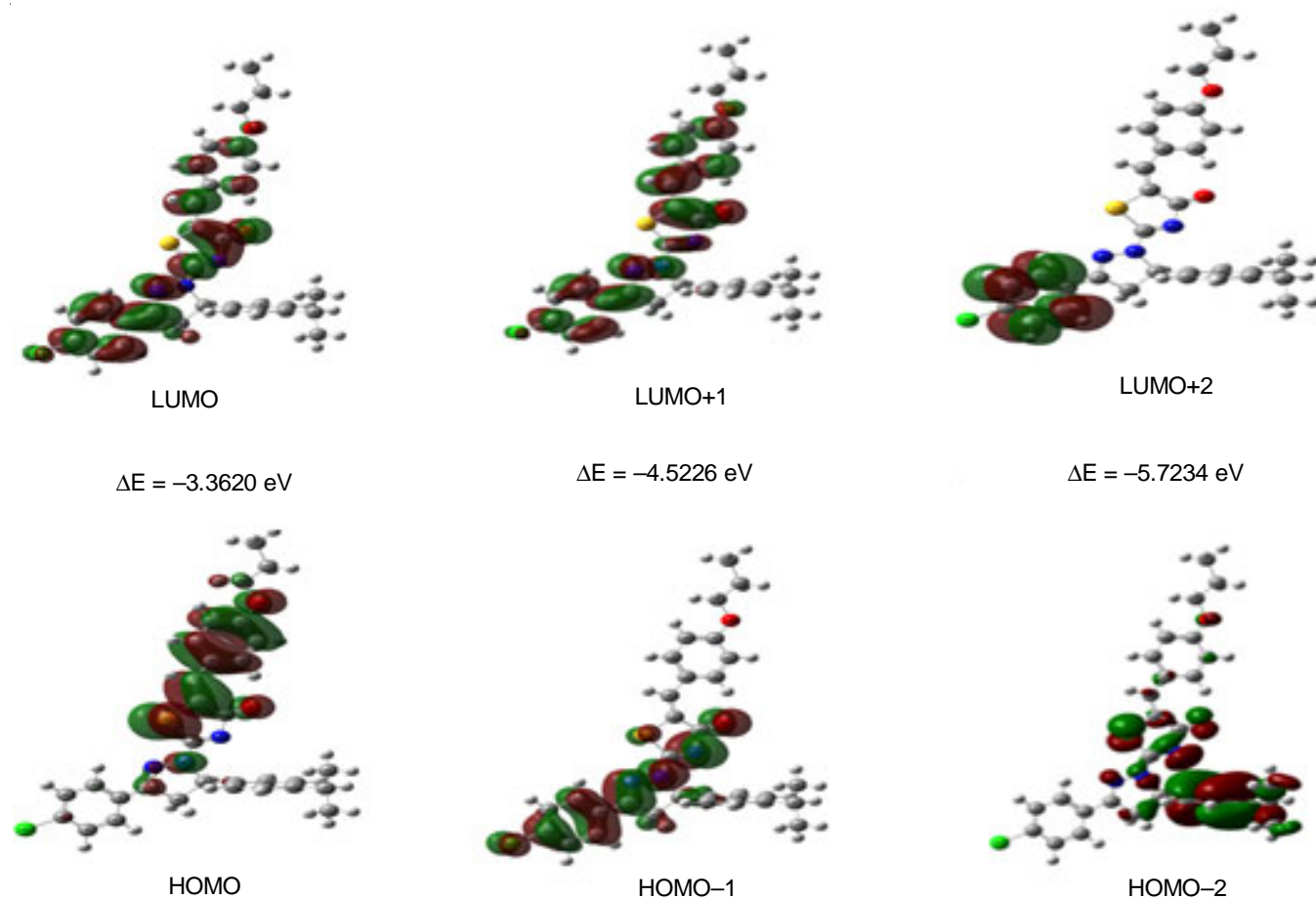


Fig. 4. HOMO-LUMO energy distribution plots of 5-(4-propoxybenzylidene)-2-[3-(4-chlorophenyl)-5-[4(propan-2-yl)phenyl]-4,5-dihydro-1*H*-pyrazol-1-yl]-1,3-thiazol-4(5*H*)-one at DFT/6-311G basis set

TABLE-3
CALCULATED E-HOMO, E-LUMO(H-1 \rightarrow L+1, H-2 \rightarrow L+2), ENERGY GAP ($E_{\text{L}}-E_{\text{H}}$), IONIZATION POTENTIAL (I), ELECTRON AFFINITY (A), GLOBAL HARDNESS (η), ELECTRONEGATIVITY (χ), CHEMICAL SOFTNESS (σ), CHEMICAL POTENTIAL (μ) AND GLOBAL ELECTROPHILICITY (ω) USING THE 6-311G LEVELS OF THEORY

Molecular properties	Energy (eV)	Energy gap (eV)	I (eV)	A (eV)	η (eV)	χ (eV)	σ (eV)	μ (eV)	ω (eV)
E_{HOMO}	-5.7563								
E_{LUMO}	-2.3943	3.3620	5.7563	2.3943	1.6810	4.753	0.5949	-4.0753	4.9399
$E_{\text{HOMO-1}}$	6.3539								
$E_{\text{LUMO+1}}$	1.8313	4.5226	6.3539	1.8313	2.2613	4.0926	0.4422	-4.0926	3.7035
$E_{\text{HOMO-2}}$	6.7645								
$E_{\text{LUMO+2}}$	1.0411	5.7234	6.7645	1.0411	2.8617	3.9028	0.3494	-3.9028	2.6613

reactions. The electrostatic potential $V(r)$ is identified as the energy collaborated between the charges formed by protons, electrons and nuclei existing in a given dimension [34,35]. We have reported and plotted the MEP surface mapping density of the title compound using Gaussian 09 program [8]. Potential increases in the order red < orange < yellow < green < blue. The negative (red and yellow) regions of MEP were related to electrophilic reactivity and the positive (green and blue) regions to nucleophilic reactivity. From the MEP, it is evident that the negative charge covers the carbonyl group is located on the thiazol ring and propoxybenzylidene, positive charge covers all hydrogen atoms in the molecule and then the neutral region is located over the remaining groups. The molecular electrostatic potential surface of the title compound is shown in Fig. 5.

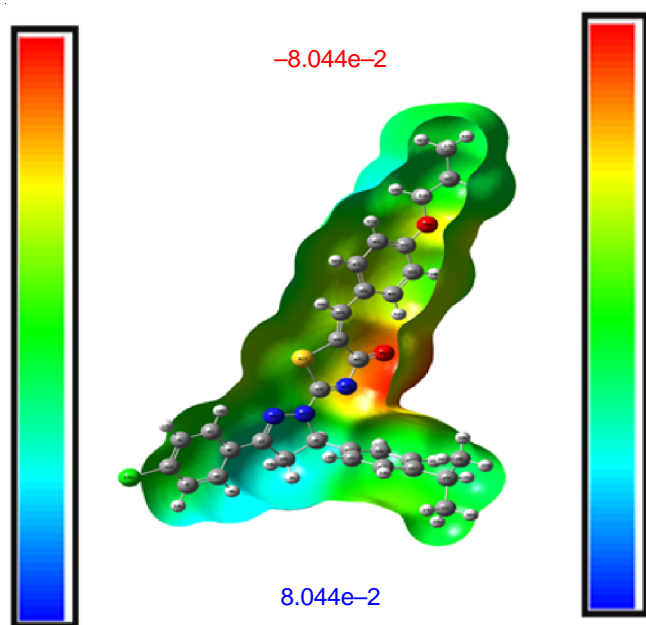


Fig. 5. MEP (molecular electrostatic potential surface) of 5-(4-propoxybenzylidene)-2-[3-(4-chlorophenyl)-5-[4(propoxy-2-yl)phenyl-4,5-dihydro-1*H*-pyrazol-1-yl]-1,3-thiazol-4(5*H*)-one

NBO analysis: Natural bond orbital analysis [11] gives an understanding of the intermolecular and intramolecular interactions of atomic bonds leading to the stability of the molecule. This analysis is carried out by examining all possible interactions between “filled (donor) Lewis-type NBOs and “empty” (acceptor) non-Lewis NBOs, estimating their energetic importance by second-order perturbation theory. The NBO analysis allows the measuring of the hybridization of atoms involved in bonding orbitals and of the atomic lone pairs. Moreover, this type gives as BD (1) for 1-center bond, BD (2) for 2-center bond, LP (1) for 1-center valence lone pair and BD*(1) for 1-center anti-bond, BD*(2) for 2-center anti-bond labels corresponding to Lewis and non-Lewis NBOs, respectively. For each donor (i) and acceptor (j), the stabilization energy $E(2)$ associated with the delocalization $i \rightarrow j$ is estimated as eqn. 1:

$$E(2) = \Delta E_{ij} = q_i \frac{(F_{ij})^2}{(E_j - E_i)} \quad (1)$$

where q_i is the donor orbital occupancy, E_i and E_j are diagonal elements and $F(i,j)$ is the off-diagonal NBO element. The intramolecular charge transfer interactions for the most significant stabilization energies $E(2)$ were obtained from the NBO calculations. The larger the $E(2)$ value shows the intensive interaction between electron-donors, electron-acceptors and the greater extent of conjugation [36,37] of the whole system are presented in Table-4. The most important hyper conjugative interaction of the title compound is bonding to lone pair BD (2) C39-C45 \rightarrow LP (2) S41 shows the leading stabilization energy of 540.23 kcal/mol. The delocalization of BD*(2) electron from anti-bonding distributed to anti-bonding show the high stabilization energy is BD*(2) C7-C11 \rightarrow BD*(2) C6-C9 for 131.61 kcal/mol and BD*(2) C7-C11 \rightarrow BD*(2) C4-C5 for 195.69 kcal/mol. Lone pair of sulphur LP (2) S41 is distributed to anti-bonding BD*(1) C42-N43 and BD*(1) C39-C45 show the stabilization energy of 99.8 kcal/mol and 65.6 kcal/mol. This electron energy has been observed and listed in Table-4 as a result of occupational interaction.

Topology analysis

Atoms in molecules (AIM): The quantum theory of atoms in molecules (AIM) is a useful tool for the characterization of hydrogen bonding, and intramolecular interactions within the molecule [38,39]. The chemical structure of an element is identified using critical point's (CP's). The type of critical point described as: (3, -3) nuclear critical point (NCP); (3, -1) bond critical point (BCP); (3, +1) ring critical point (RCP); and (3,+3) cage critical point (CCP). The number and type of critical points that can coexist in a molecule or crystal follow a strict topological relationship which states eqn. 2 as:

$$n_{\text{NCP}} - n_{\text{BCP}} + n_{\text{RCP}} - n_{\text{CCP}} = \begin{cases} 1(\text{Isolated-molecules}) \\ 0(\text{Infinite-crystals}) \end{cases} \quad (2)$$

where n denotes the number of the subscripted type of CP. The topology relationship of an isolated system is known as the Poincare-Hopf (PH) relationship. The topology analysis of the compound displays 68 (3,-3) nuclear critical points, 73 (3,-1) bond critical points (BCPs) between attractive pairs and 6 (3,+1) ring critical points corresponding to π - π interactions. One bond critical point is associated with a very weak (O44-C40-C39-C45-C45-C48 -H52) hydrogen bonding interaction. When these lines show that the Poincare-Hopf relationship is satisfied, we can see all expected CPs are presented, hence we can confirm that all CPs have been found.

$$(3, -3): 68, (3, -1): 73, (3, +1): 6, (3,+3): 0 \\ 68 - 73 + 6 - 0 = 1$$

From Multiwfn, the energy of hydrogen bond is calculated by a relationship between bond energy E_{HB} (eqn. 3) and potential energy density $V(r_{\text{BCP}})$ at corresponding BCP as:

$$E_{\text{HB}} = \frac{V(r_{\text{BCP}})}{2} \quad (3)$$

The energy of the hydrogen bond O44-C40-C39-C45-C46-C48 -H52 was calculated to be 46.60 kcal/mol. Magenta, orange and yellow spheres correspond to (3, -3), (3, -1) and (3, +1) critical points and bond path Fig. 6(A). The indices of CPs are labelled by cyan numbers. The yellow sphere and line

TABLE-4
SECOND ORDER PERTURBATION THEORY ANALYSIS OF FOCK MATRIX ON NBO OF THE 5-(4-PROPOXYBENZYLIDENE)-2-[3-(4-CHLOROPHENYL)-5-[4-(PROPAN-2-YL)PHENYL]-4,5-DIHYDRO-1*H*-PYRAZOL-1-YL]-1,3-THIAZOL-4(5*H*)-ONE

Donar (i)	Type	ED/e	Acceptor (j)	Type	ED/e(q)	E(2) ^a (Kcal/mol)	E(i)-E(j) ^b	F(i,j) ^c
BD (2)	C1-N24	1.92317	BD*(2)	C4-C5	0.38999	7.93	0.32	0.049
BD (1)	C1-C26	1.97344	BD*(1)	C2-C14	0.03967	5.08	1.09	0.067
BD (1)	C2-H55	1.89423	BD*(1)	H3-C26	0.04766	8.32	0.91	0.079
BD (2)	C4-C5	1.64504	BD*(2)	C1-N24	0.2551	16.67	0.24	0.058
BD (2)	C4-C5	1.64504	BD*(2)	C6-C9	0.29685	19.66	0.28	0.068
BD (2)	C4-C5	1.64504	BD*(2)	C7-C11	0.39233	22.43	0.26	0.069
.BD (1)	C6-C9	1.64504	BD*(1)	C11-C127	0.03193	4.95	0.81	0.057
.BD (2)	C6-C9	1.66679	BD*(2)	C4-C5	0.38999	20.57	0.28	0.068
.BD (2)	C6-C9	1.66679	BD*(2)	C7-C11	0.39233	21.12	0.26	0.067
BD (2)	C7-C11	1.67977	BD*(2)	C4-C5	0.38999	17.84	0.3	0.066
BD (2)	C7-C11	1.67977	BD*(2)	C6-C9	0.29685	19.15	0.3	0.068
BD (2)	C14-C15	1.67260	BD*(2)	C16-C19	0.34331	19.55	0.28	0.067
BD (2)	C14-C15	1.67260	BD*(2)	C17-C21	0.35910	18.95	0.29	0.067
BD (2)	C16-C19	1.69329	BD*(2)	C14-C15	0.38842	21.07	0.27	0.069
BD (2)	C16-C19	1.69329	BD*(2)	C17-C21	0.35910	21.11	0.28	0.07
BD (2)	C17-C21	1.64966	BD*(2)	C14-C15	0.38842	21.43	0.27	0.069
BD (2)	C17-C21	1.64966	BD*(2)	C16-C19	0.34331	20.03	0.28	0.066
BD (1)	C29-H38	1.90958	BD*(2)	C17-C21	0.35910	10.97	0.47	0.069
BD (1)	C29-H38	1.90958	BD*(1)	C30-H34	0.01540	6.13	0.93	0.069
BD (1)	C29-H38	1.90958	BD*(1)	C31-H37	0.01540	6.13	0.93	0.069
BD (1)	C39-S41	1.97750	BD*(1)	N25-C42	0.05342	9	1.44	0.102
BD (2)	C39-C45	1.72685	LP (2)	S41	1.99791	540.23	0.01	0.119
BD (2)	C39-C45	1.72685	BD*(2)	C40-O44	0.35800	29.54	0.28	0.083
BD (1)	C40-N43	1.98023	BD*(1)	N25-C42	0.05342	6.25	1.17	0.077
BD (2)	C40-O44	1.91570	BD*(2)	C39-C45	0.28406	8.91	0.27	0.046
BD (2)	C40-O44	1.91570	BD*(2)	C42-N43	0.51724	6.73	0.28	0.044
BD (1)	S41-C42	1.98222	BD*(1)	C39-C45	0.03534	7.14	1.39	0.089
BD (1)	C42-N43	1.97971	BD*(1)	S41-C42	0.04637	1.15	1.29	0.035
BD (2)	C42-N43	1.83934	LP (2)	S41	1.99791	102.39	0.05	0.102
BD (2)	C42-N43	1.83934	BD*(2)	C40-O44	0.35800	27.11	0.31	0.087
BD (2)	C46-C48	1.66946	BD*(2)	C47-C49	0.31590	20.72	0.29	0.069
BD (2)	C46-C48	1.66946	BD*(2)	C51-C53	0.35490	19.28	0.28	0.066
BD (2)	C47-C49	1.66513	BD*(2)	C46-C48	0.36800	20.58	0.27	0.068
BD (2)	C47-C49	1.66513	BD*(2)	C51-C53	0.35490	22.37	0.27	0.07
BD (2)	C51-C53	1.65032	BD*(2)	C46-C48	0.36800	21.42	0.28	0.07
BD (2)	C51-C53	1.65032	BD*(2)	C47-C49	0.31590	19.26	0.29	0.067
LP (1)	N24	1.99950	BD*(1)	C2-N25	0.04392	4.81	0.82	0.056
LP (1)	N25	1.99906	BD*(2)	C1-N24	0.25510	26.7	0.24	0.072
LP (1)	N25	1.99906	BD*(1)	S41-C42	0.04637	6.95	0.75	0.068
LP (1)	N25	1.99906	BD*(1)	C42-N43	0.06186	13.04	0.68	0.088
LP (3)	C127	1.99995	BD*(2)	C7-C11	0.39233	12.39	0.32	0.061
LP (1)	S41	2.00000	BD*(1)	C39-C40	0.09667	7.95	0.99	0.08
LP (1)	S41	2.00000	BD*(1)	C42-N43	0.06186	8.55	0.94	0.08
LP (2)	S41	1.99791	BD*(2)	C39-C45	0.03534	65.6	0.2	0.112
LP (2)	S41	1.99791	BD*(2)	C42-N43	0.51724	99.8	0.21	0.133
LP (1)	N43	1.99941	BD*(1)	C39-C40	0.09667	5.99	0.81	0.062
LP (1)	N43	1.99941	BD*(1)	S41-C42	0.04637	5.63	0.84	0.062
LP (2)	O44	1.87708	BD*(1)	C39-C40	0.09667	18.59	0.69	0.102
LP (2)	O44	1.87708	BD*(1)	C40-N43	0.06186	22.97	0.65	0.111
LP (1)	O58	1.94538	BD*(1)	C49-C53	0.02868	6	0.97	0.069
BD*(2)	C1-N24	0.25510	BD*(2)	C4-C5	0.38999	37.71	0.04	0.063
BD*(2)	C7-C11	0.39233	BD*(2)	C4-C5	0.38999	195.69	0.02	0.083
BD*(2)	C7-C11	0.39233	BD*(2)	C6-C9	0.29685	131.61	0.02	0.078
BD*(2)	C39-C45	0.03534	BD*(2)	C40-O44	0.35800	30.02	0.06	0.069
BD*(2)	C42-N43	0.51724	BD*(2)	C40-O44	0.35800	53.08	0.05	0.072

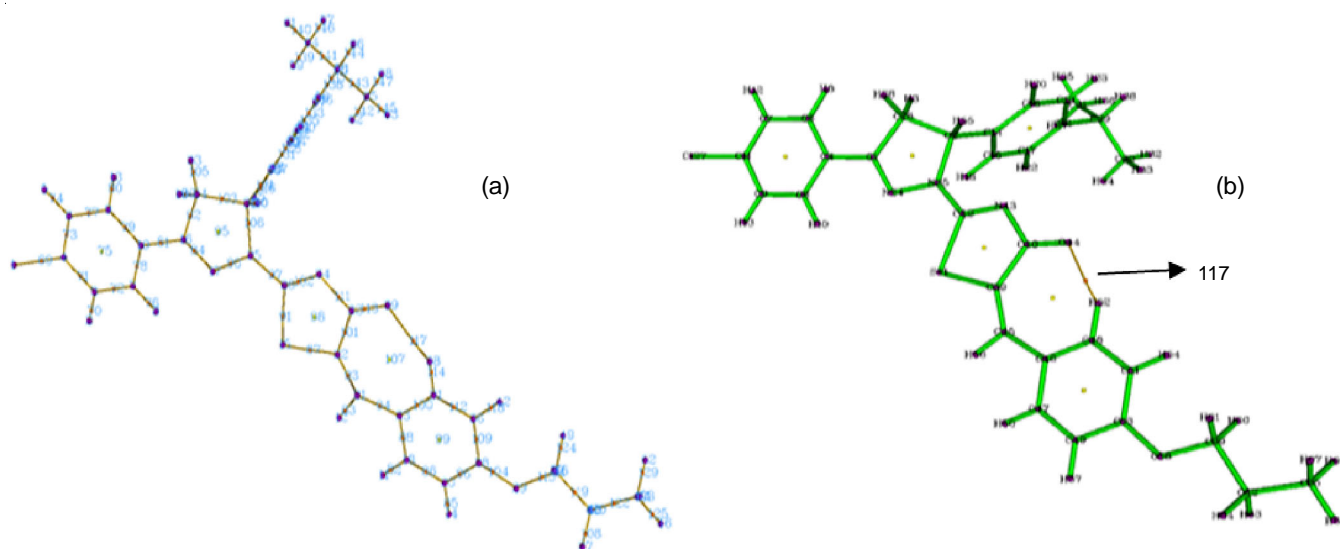


Fig. 6. AIM critical point maps of the 5-(4-propoxybenzylidene)-2-[3-(4-chlorophenyl)-5-[4(propan-2-yl)phenyl]-4,5-dihydro-1*H*-pyrazol-1-yl]-1,3-thiazol-4(5*H*)-one bonding region

denote between the green colour bond path show the index 117 corresponds to the bond critical point (BCP) of O-C...H hydrogen bond, respectively. AIM map of the hydrogen bonding region are presented in Fig. 6b.

Localized orbital locator (LOL) and electron localization function (ELF): The topologies of the localized orbital locator (LOL) and electron localization function (ELF) are investigated electron density (gradient) in an attempt to elucidate cores and the valence shell of the atoms. To define Fermi hole curvature Becke & Edgecombe [40] proposed a local scalar function $V(r)$ and show the excess kinetic energy of the Pauli repulsion regions (absence of LOL) of space. Extensively, Savin & Silvi [41] explained the two main types of basins in a molecule: core and valence. Core basins engulf centre nuclei present in the molecule and valence basins identifies the boundaries shared by the cores and lone pair. The localized orbital locator (LOL) shows the surface topology of interaction bond path. The carbon and nitrogen core present in compound is represented by the red-dot blue ring, inner shell is represented by red-dot yellow ring and the path electrons delocalization is

represented by greenish-yellow colour shown in Fig. 7a. The axis's of the LOL limits from 0.00 to 1.00. ELF isosurface explains the relation between LOL and ELF regions of the title compound is shown in Fig. 7b. From electron localization function (ELF) analysis, it finds the positions of isosurface, shared and unshared in space where ELF is maximal and to use the value of ELF in these points. By defining the electron localization (ELF) gradient in terms of η by the mapping its values on to range $0 \leq \eta \leq 1$: The value of ELF, $\eta(r)$ ranges from 0.0 to 1.00, where relatively high values in the interval 1.00 to 0.5 indicates regions containing bonding and anti-bonding localized electrons, whereas lower values (> 0.5) describe domains where electrons are expected to be delocalized. Very low electron localization zones between valence and inner shells revealed by the blue ring like region around each carbon and nitrogen atoms. Next, high electron localization zones between core and lone pair to valence atoms are revealed by the red ring like region around each hydrogen, chlorine (LP) and oxygen (LP) atoms. Colour shade maps or contour maps of bonding region are present in Fig. 7c. High ELF values

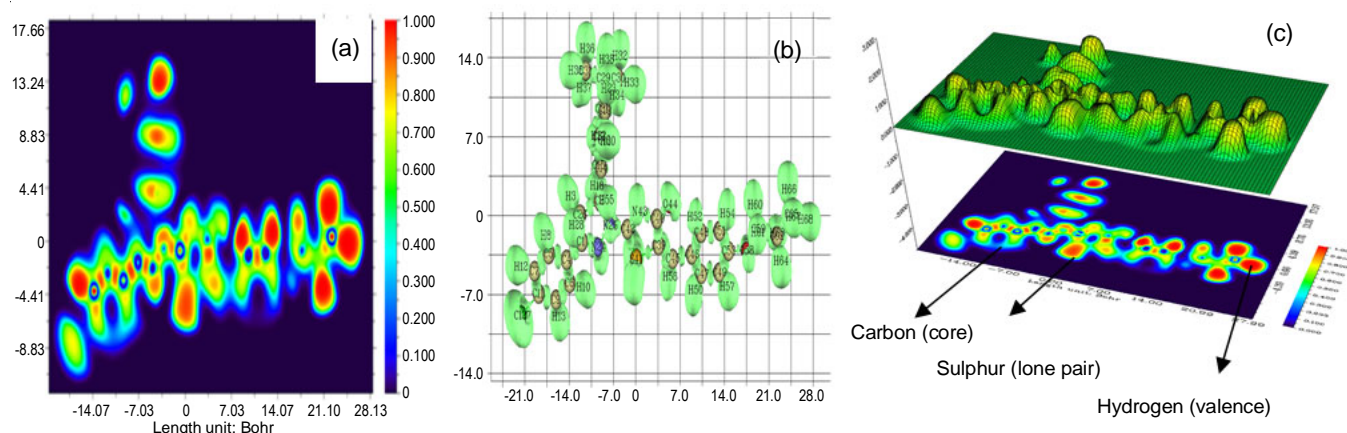


Fig. 7. (a) LOL, (b) ELF isosurface and (c) ELF region of 5-(4-propoxybenzylidene)-2-[3-(4-chlorophenyl)-5-[4(propan-2-yl)phenyl]-4,5-dihydro-1*H*-pyrazol-1-yl]-1,3-thiazol-4(5*H*)-one

(~ 0.600 to 1.00 Bohr unit) are coloured red; the series descends through yellow to green for middle (0.60 to 0.40 Bohr unit) and the lower end (below 0.4 Bohr unit) of the scale is represented by blue.

Reduced density gradient analysis (RDG): Recently developed the non-covalent interactions (NCI) method to detect NCI in real space [42]. This method enables the identification of NCI as isosurfaces of the reduced density gradient RDG (r) in eqn. 4:

$$RDG(r) = \frac{1}{2(3\pi^2)^{1/2}} \frac{|\nabla\rho(r)|}{\rho(r)^{4/3}} \quad (4)$$

These isosurfaces expand over large regions of space containing interacting atoms. This approach recovers a more intuitive picture of van der Waals interactions, hydrogen bonds and steric repulsions than other local pair wise approaches, such as atoms in molecules (AIM) theory, or the electron localization function (ELF). The application of the reduced density gradient is to visualize interacting regions was motivated by the deviations from the exponential behaviour observed when RDG is plotted *versus* $\rho(r)$ for interacting systems [43]. Value of Hessian matrix of electron density is used to find the nature of an interaction. If $\lambda_2 > 0$, for non-bonded and if $\lambda_2 < 0$ for bonded. The blue colour indicates the hydrogen bonding interaction, the green colour represents van der Waals interactions and the red colour is identified as strong repulsion. From Fig. 8, the van der Waals interaction is the predominant factor as electrostatic interaction in the molecule. The isosurface of the title compound displays very strong van der Waals interact with strong steric effect as repulsive interaction and weak hydrogen bonding (one only) interaction. Moreover, hydrogenic and van der Waals regions are more impacted in the presence of propoxybenzylidene moiety in the structure pyrazole and thiazole.

Molecular docking: To explore the biological activity of the title molecule, molecular docking simulations have been performed using Auto Dock/Vina software [44]. Docking has

become a standard technology in drug discovery to virtually screen hypothetical chemicals to identify new active chemotypes, which predicts the target binding modes of protein and to point out the active site of ligands. PASS [45] is an online tool that predicts different types of activities based on the compound structure. From PASS analysis of title compound predicts several activities, amongst other activities choosing Pim-1 kinase inhibitor activity with Pa (probability to be active) and Pi (probability to be inactive) values are listed in Table-5. In light of their oncogenic potential, the Pim kinase family is

Pa	Pi	Activity name
0.260	0.102	Antimetastatic
0.189	0.036	Pim-1 kinase inhibitor
0.177	0.031	Protein-tyrosine phosphatase inhibitor
0.153	0.012	Bcl2 antagonist
0.192	0.054	Vascular adhesion protein 1 inhibitor
0.133	0.008	Pim-2 kinase inhibitor
0.242	0.121	Atherosclerosis treatment
0.246	0.131	Antineurogenic pain
0.101	0.005	CDC25B inhibitor
0.107	0.018	Autotaxin inhibitor
0.128	0.039	Lipoxygenase inhibitor
0.292	0.205	APOA1 expression enhancer
0.207	0.120	Antiobesity
0.132	0.049	Vasculitis treatment
0.082	0.010	Bcl-xL inhibitor
0.126	0.061	Sodium/bile acid cotransporter inhibitor
0.093	0.030	5-Lipoxygenase inhibitor
0.260	0.199	CDK9/cyclin T1 inhibitor
0.078	0.024	Protein-tyrosine phosphatase 2C inhibitor
0.205	0.157	Antidiabetic
0.092	0.044	Peroxisome proliferator-activated receptor gamma antagonist
0.240	0.195	Vanilloid 1 agonist

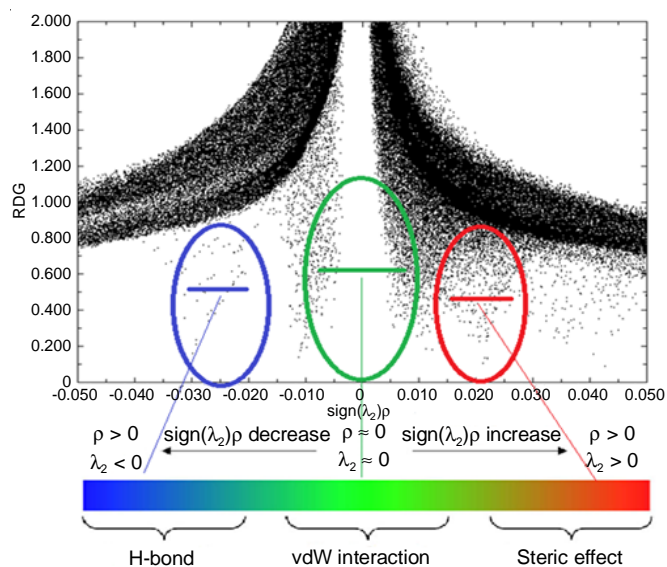


Fig. 8. Reduced density gradient 2D and 3D of 5-(4-propoxybenzylidene)-2-[3-(4-chlorophenyl)-5-[4(propan-2-yl)phenyl]-4,5-dihydro-1H-pyrazol-1-yl]-1,3-thiazol-4(5H)-one

emerging as an important new target for drug discovery efforts. Pim kinases are emerging as important mediators of cytokine signaling pathways in hematopoietic cells and they contribute to the progression of certain leukemias and solid tumors [46]. Based on this, molecular docking simulation was carried out for the title compound bind with the human Pim-1 kinase enzyme. The 3D structure of proteins was obtained from Protein Data Bank (PDB ID: 3A99, 1GJ8, 1XQZ) has a good resolution. Auto Dock Tools (ADT) graphical user interface was used to add polar hydrogen and to calculate atomic charges by Kollman method. Water molecules and co-crystallized ligands were removed. The optimized structures of ligands PDB were obtained using the DFT (B3LYP) theory with the 6-311G basis set on Gaussian 09. Partial charges were calculated by Geistenger method. The active site to the energies was defined to add residues of the active site with the use of grid size 126 Å × 126 Å × 126 Å using Auto grid [47]. The Auto Dock binding affinity (kcal/mol), inhibition constants (nM or μM) and nature of the bond with residues were computed (Table-6) and the best lowest energy docked position of the ligand with target protein are shown in Figs. 9a-b. The bond interactions present in the title compound are pi-alkyl, carbon-hydrogen bond,

conventional hydrogen bond and pi-cation, 3A99 interaction with amino acid forms alkyl (2.5 Å; ILE A:74, 3.0 Å; VAL A:174) having various binding energies of -9.23, -9.13 and -9.01 kcal/mol. The inhibition constant values are identified as 170.15 nM, 201.86 nM, 248.98 nM and RMSD value are 81.47 Å, 83.69 Å and 82.21 Å. The result of 1GJ8 encircled by residues pi-sigma (2.8 Å, CYS A:13), conventional hydrogen bond (1.9 Å, GLN A:12) and alkyl (2.9 Å, LYS A:10). They have a docking score of -6.98, -6.95, -6.90 kcal/mol, respectively. The inhibition constant values are identified as 7.65 μM, 19.13 μM and 12.09 μM and RMSD value are 26.16 Å, 26.28 Å and 26.31 Å. The prediction of 1XQZ insight the potent of Pim kinase inhibitor docked with ligand shows van der Waals (2.6 Å, GLN A :171), alkyl (2.4 Å, PRO A:125; 2.4 Å, LEU A: 93; 2.4 Å, LYS A: 67), which can provide some binding energies of -9.14, -9.01 and -7.83 kcal/mol. The inhibition constant values are identified as 201.35 nM, 249.97 nM and 1.82 μM. The RMSD value is 77.89 Å, 79.25 Å and 55.22 Å.

Conclusion

The FT-IR and FT-Raman spectra of 5-(4-propoxybenzylidene)-2-[3-(4-chlorophenyl)-5-[4-(propan-2-yl)phenyl]-4,5-

TABLE-6
MOLECULAR DOCKING PARAMETERS OF 5-(4-PROPOXYBENZYLIDENE)-2-[3-(4-CHLOROPHENYL)-5-[4-(PROPAN-2-YL)PHENYL]-4,5-DIHYDRO-1H-PYRAZOL-1-YL]-1,3-THIAZOL-4(5H)-ONE BIND WITH HUMAN PIM-1 KINASE ENZYME

PDB ID	Bond distance (Å)	Amino acid (residues)	Bond	Binding affinity (kcal/mol)			Inhibition constant Ki (μM or nM)			RMSD (Å)		
				1	2	3	1	2	3	1	2	3
3A99	2.5	ILE A 74	Pi-alkyl									
	2.9	GLY A 48	Carbon-hydrogen bond									
	3.0	SER A 50	Conventional hydrogen bond	-9.23	-9.13	-9.01	170.15 nM	201.86 nM	248.98 nM	81.47	83.69	82.21
	3.0	VAL A 174	Pi-alkyl									
1GJ8	2.8	CYS A 13	Pi-sigma									
	1.9	GLN A 12	Conventional hydrogen bond	-6.98	-6.95	-6.90	7.65 μM	19.13 μM	12.09 μM	26.16	26.28	26.31
	2.9	LYS A 10	Alkyl									
1XQZ	2.6	GLN A 171	Van der Waals									
	2.4	PRO A 125	Pi-alkyl									
	2.4	LEU A 93	Pi-alkyl	-9.14	-9.01	-7.83	201.35 nM	249.97 nM	1.82 μM	77.89	79.25	55.22
	2.4	LYS A 67	Pi-alkyl									
	3.5	ILE A 185	Pi-sigma									

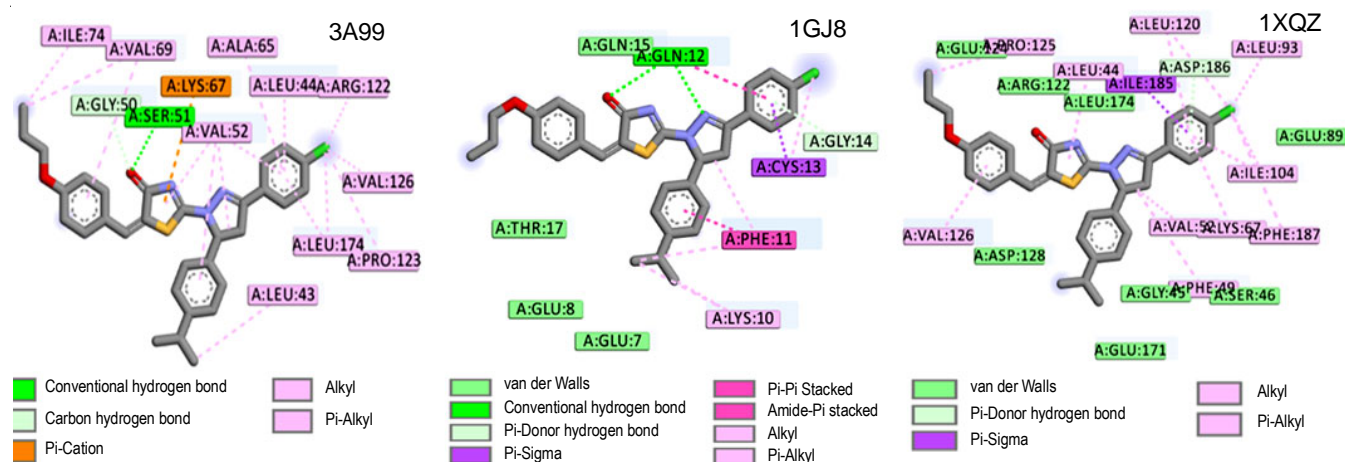


Fig. 9a. Residues interactions of Pim-1 kinase inhibitor protein with ligand (PCPPT)

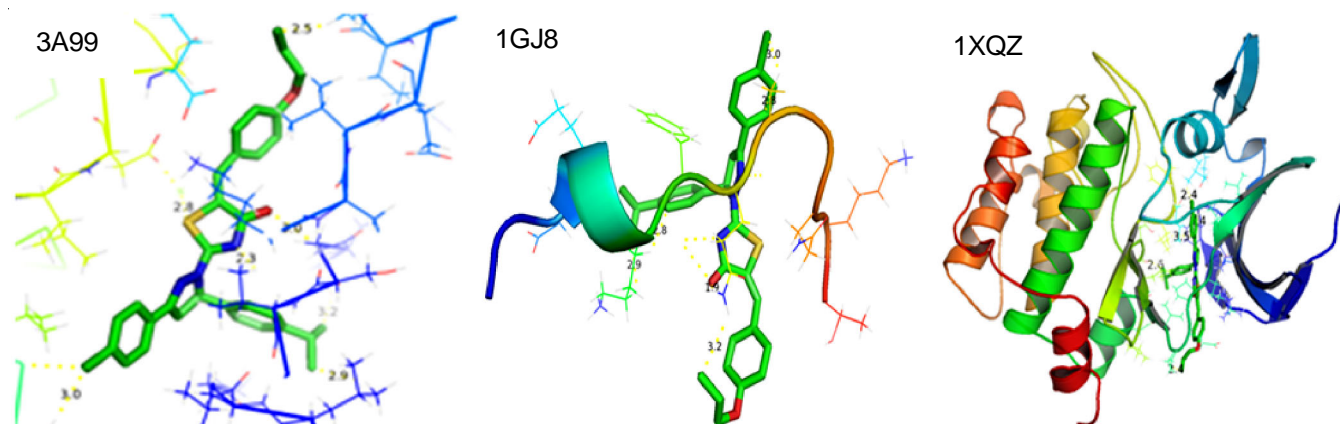


Fig. 9b. Docked position values of Pim-1 kinase inhibitor protein with ligand (PCPPT)

dihydro-1*H*-pyrazol-1-yl]-1,3-thiazol-4(5*H*)-one was studied by both experimentally and theoretically. The vibrational wavenumber was computed using B3LYP/6-31G and B3LYP/6-311G basis sets DFT methods are assigned with the help of potential energy distribution analysis. The HOMO and LUMO analysis are used to determine the charge transfer and the chemical activity of molecule. From the molecular electrostatic potential, it is evident that the negative charge covers the carbonyl group, positive charge covers hydrogen atoms in the propoxybenzylidene, the neutral region is covered over the remaining groups and show the more electronegativity in the carbonyl group makes it the most reactive part of the compound. The stability of the molecule arising from hyperconjugative interaction and charge delocalization has been studied using NBO analysis. AIM confirms the presence of an intramolecular hydrogen bond between O44-H27...N14 with energy of 46.60 kcal/mol. The surface electron density core, lone pair and valence findings were confirmed by electron localization function (ELF) and localized orbital locator (LOL) studies. Intra- and intermolecular non-covalent and weak interactions (van der Waals forces) of thiazole and pyrazole were explored using the reduced density gradient (RDG) methods. The anticancerous protein 3A99 is having higher binding energy, inhibition constant and RMSD values such as -9.23 kcal/mol, 170.15 nM and 81.47 Å than 1GJ8 1XQZ. From the results, the title compound may be observed as an effective Pim-1 kinase drug.

CONFLICT OF INTEREST

The authors declare that there is no conflict of interests regarding the publication of this article.

REFERENCES

- P. Blum, A. Sagner, A. Tiehm, P. Martus, T. Wendel and P. Grathwohl, *J. Contam. Hydrol.*, **126**, 181 (2011); <https://doi.org/10.1016/j.jconhyd.2011.08.004>
- Y.S. Mary, C.Y. Panicker, M. Sapnakumari, B. Narayana, B.K. Sarojini, A.A. Al-Saadi, C.V. Alsenoy and J.A. War, *Spectrochim. Acta A Mol. Biomol. Spectrosc.*, **136**, 483, (2015); <https://doi.org/10.1016/j.saa.2014.09.061>
- G. Susithra, S. Ramalingam, S. Periandy and R. Aarthi, *Egypt. J. Basic Appl. Sci.*, **4**, 313 (2018); <https://doi.org/10.1016/j.ejbas.2018.05.011>
- S. Aayisha, T.S.R. Devi, S. Janani, S. Muthu, M. Raja, S. Sevvanthi and R. Hemamalini, *Comput. Biol. Chem.*, **86**, 107226 (2020); <https://doi.org/10.1016/j.compbiolchem.2020.107226>
- I.W. Cheney, S. Yan, T. Appleby, H. Walker, T. Vo, N. Yao, R. Hamatake, Z. Hong and J.Z. Wu, *Bioorg. Med. Chem. Lett.*, **17**, 1679 (2007); <https://doi.org/10.1016/j.bmcl.2006.12.086>
- D. Morishita, M. Takami, S. Yoshikawa, R. Katayama, M. Kukimoto-Niino, S. Sato, T. Umehara, M. Shirouzu, K. Sekimizu, S. Yokoyama and N. Fujita, *J. Biol. Chem.*, **286**, 2681 (2011); <https://doi.org/10.1074/jbc.M109.092452>
- V. V. Salian, B.K. Narayana, B.K. Sarojini, M.S. Kumar and A.G. Lobo, *J. Mol. Struct.*, **1192**, 91 (2019); <https://doi.org/10.1016/j.molstruc.2019.04.105>
- M.J. Frisch, G.W. Trucks, H.B. Schlegel, G.E. Scuseria, M.A. Robb, J.R. Cheeseman, G. Scalmani, V. Barone, B. Mennucci, G.A. Petersson, H. Nakatsuji, M. Caricato, X. Li, H.P. Hratchian, A.F. Izmaylov, J. Bloino, G. Zheng, J.L. Sonnenberg, M. Hada, M. Ehara, K. Toyota, R. Fukuda, J. Hasegawa, M. Ishida, T. Nakajima, Y. Honda, O. Kitao, H. Nakai, T. Vreven, J.A. Montgomery, Jr., J.E. Peralta, F. Ogliaro, M. Bearpark, J.J. Heyd, E. Brothers, K.N. Kudin, V.N. Staroverov, R. Kobayashi, J. Normand, K. Raghavachari, A. Rendell, J.C. Burant, S.S. Iyengar, J. Tomasi, M. Cossi, N. Rega, J.M. Millam, M. Klene, J.E. Knox, J.B. Cross, V. Bakken, C. Adamo, J. Jaramillo, R. Gomperts, R.E. Stratmann, O. Yazyev, A.J. Austin, R. Cammi, C. Pomelli, J.W. Ochterski, R.L. Martin, K. Morokuma, V.G. Zakrzewski, G.A. Voth, P. Salvador, J.J. Dannenberg, S. Dapprich, A.D. Daniels, Ö. Farkas, J.B. Foresman, J.V. Ortiz, J. Cioslowski and D.J. Fox, Gaussian 09, Gaussian, Inc., Wallingford CT (2009).
- R. Dennington, T. Kerth and J. Millam, Gauss View, Version 5.0, Semicham. Inc., Shawnee Mission KS (2009).
- M.H. Jamroz, *Spectrochim. Acta A Mol. Biomol. Spectrosc.*, **114**, 220 (2013); <https://doi.org/10.1016/j.saa.2013.05.096>
- T. Lu and F. Chen, *J. Comput. Chem.*, **33**, 580 (2011); <https://doi.org/10.1002/jcc.22885>
- E.D. Glendening and A.E. Reed, NBO Version 3.1, TCL, University of Wisconsin, Madison, USA (1998). <https://www.pymol.org>
- Biovia discovery studio 4.5; <https://discover.3ds.com>
- S. Parveen, M.A. Al-Alshaikh, C.Y. Panicker, A.A. El-Emam, B. Narayana, V. V. Saliyan and C. Van Alsenoy, *J. Mol. Struct.*, **1112**, 136 (2016); <https://doi.org/10.1016/j.molstruc.2016.02.018>
- A.S. Devi, V.V. Aswathy, Y.S. Mary, C.Y. Panicker, S. Armakovic, S.J. Armakovic and C. Van Alsenoy, *J. Mol. Struct.*, **1148**, 282 (2017); <https://doi.org/10.1016/j.molstruc.2017.07.065>
- K. Venil, A. Lakshmi, V. Balachandra, B. Narayana and V.V. Salian, *J. Mol. Struct.*, **1225**, 129070 (2021); <https://doi.org/10.1016/j.molstruc.2019.127394>
- Y.S. Mary, C.Y. Panicker, S. Armakovic, S.J. Armakovic, B. Narayana, B.K. Sarojini and C. Van Alsenoy, *J. Mol. Struct.*, **1148**, 266 (2017); <https://doi.org/10.1016/j.molstruc.2017.07.052>

19. R.A. Sheakh Mohamad, W.M. Hamad and H.J. Aziz, *Acta Cryst.*, **E76**, 920 (2020); <https://doi.org/10.1107/S2056989020006611>
20. H. Behbehani and H.M. Ibrahim, *Molecules*, **17**, 6362 (2012); <https://doi.org/10.3390/molecules17066362>
21. S. Alturk, D. Avci, O. Tamer and Y. Atalay, *Comput. Theor. Chem.*, **1100**, 34 (2017); <https://doi.org/10.1016/j.comptc.2016.12.007>
22. N. Colthup, Introduction to Infrared and Raman Spectroscopy, Elsevier (2012).
23. B. Smith, Infrared Spectral Interpretation: A Systematic Approach, CRC Press, Washington, DC (1999).
24. A.Viji, V. Balachandran, S. Babiyana, B. Narayana and V.V. Saliyan, *J. Mol. Struct.*, **1215**, 128244 (2020); <https://doi.org/10.1016/j.molstruc.2020.128244>
25. V. Arjunan, R. Anitha, S. Thirunarayanan and S. Mohan, *Chem. Data Coll.*, **11-12**, 139 (2017); <https://doi.org/10.1016/j.cdc.2017.09.002>
26. S.M. Hiremath, A. Suviha, N.R. Patil, C.S. Hiremath, S.S. Khemalapur, S. K. Pattanayak, V.S. Negalurmath and K. Obelannavar, *J. Mol. Struct.*, **1171**, 362 (2018); <https://doi.org/10.1016/j.molstruc.2018.05.109>
27. Y.B. Shankar Rao, M.V.S. Prasad, N.U. Sri and V. Veeraiah, *J. Mol. Struct.*, **1108**, 567 (2016); <https://doi.org/10.1016/j.molstruc.2015.12.008>
28. C. Sivakumar, V. Balachandran, B. Narayana, V.V. Saliyan, B. Revathi, N. Shanmugapriya and K. Vanasundari, *J. Mol. Struct.*, **1224**, 129010 (2021); <https://doi.org/10.1016/j.molstruc.2020.129010>
29. G. Socrates, *J. Chem. Educ.*, **72**, A93 (1995); <https://doi.org/10.1021/ed072pA93.5>
30. M. Kaur, Y.S. Mary, C.Y. Panicker, H.T. Varghese, H. Yathirajan, K. Byrappa and C. Van Alsenoy, *Spectrochim. Acta A Mol. Biomol. Spectrosc.*, **120**, 445 (2014); <https://doi.org/10.1016/j.saa.2013.10.032>
31. R.M. Silverstein, F.X. Webster and D. Kiemle, Spectrometric Identification of Organic Compounds, Wiley: New York, Ed.: 7 (2005).
32. Y. Sert, M. Gumus, H. Gokce, I. Kani and I. Koca, *J. Mol. Struct.*, **1171**, 850 (2018); <https://doi.org/10.1016/j.molstruc.2018.06.069>
33. R.G. Parr and R.G. Pearson, *J. Am. Chem. Soc.*, **105**, 7512 (1983); <https://doi.org/10.1021/ja00364a005>
34. E. Temel, C. Alasalvar, H. Gokce, A. Guder, C. Albayrak, Y.B. Alpaslan, G. Alpaslan and N. Dilek, *Spectrochim. Acta A Mol. Biomol. Spectrosc.*, **136**, 534 (2015); <https://doi.org/10.1016/j.saa.2014.09.067>
35. P. Koldaivel and V. Nirmala, *J. Mol. Struct.*, **694**, 33 (2004); <https://doi.org/10.1016/j.molstruc.2004.01.030>
36. A.E. Reed, L.A. Curtiss and F. Weinhold, *Chem. Rev.*, **88**, 899 (1988); <https://doi.org/10.1021/cr00088a005>
37. R.M. Asath, R. Premkumar, T. Mathavan and A.M.F. Benial, *Spectrochim. Acta A Mol. Biomol. Spectrosc.*, **175**, 51 (2017); <https://doi.org/10.1016/j.saa.2016.11.037>
38. G.L. Sosa, N.M. Peruchena, R.H. Contreras and E.A. Castro, *J. Mol. Struct.*, **577**, 219 (2002); [https://doi.org/10.1016/S0166-1280\(01\)00670-4](https://doi.org/10.1016/S0166-1280(01)00670-4)
39. E.R. Johnson, S. Keinan, P. Mori-Sanchez, J. Contreras-Garcia, A.J. Cohen and W. Yang, *J. Am. Chem. Soc.*, **132**, 6498 (2010); <https://doi.org/10.1021/ja100936w>
40. A.D. Becke and K.E. Edgecombe, *J. Chem. Phys.*, **92**, 5397 (1990); <https://doi.org/10.1063/1.458517>
41. B. Silvi and A. Savin, *Nature*, **371**, 683 (1994); <https://doi.org/10.1038/371683A0>
42. R.A. Boto, J. Contreras-García, J. Tierny and J.-P. Piquemal, *Mol. Phys.*, **114**, 1406 (2015); <https://doi.org/10.1080/00268976.2015.1123777>
43. I. Rozas, I. Alkorta and J. Elguero, *J. Am. Chem. Soc.*, **122**, 11154 (2000); <https://doi.org/10.1021/ja0017864>
44. O. Trott and A.J. Olson, *J. Comput. Chem.*, **31**, 455 (2010); <https://doi.org/10.1002/jcc.21334>
45. A. Lagunin, A. Stepanchikova, D. Filimonov and V. Poroiikov, *Bioinformatics*, **16**, 747 (2000); <https://doi.org/10.1093/bioinformatics/16.8.747>
46. A.N. Bullock, J. Debreczeni, A.L. Amos, S. Knapp and B.E. Turk, *J. Biol. Chem.*, **280**, 41675 (2005); <https://doi.org/10.1074/jbc.M510711200>
47. G.M. Morris, D.S. Goodsell, R.S. Halliday, R. Huey, W.E. Hart, R.K. Belew and A.J. Olson, *J. Comput. Chem.*, **19**, 1639 (1998); [https://doi.org/10.1002/\(SICI\)1096-987X\(19981115\)19:14<1639::AID-JCC10>3.0.CO;2-B](https://doi.org/10.1002/(SICI)1096-987X(19981115)19:14<1639::AID-JCC10>3.0.CO;2-B)